Results in Physics 43 (2022) 106107

Contents lists available at ScienceDirect

Results in Physics

journal homepage: www.elsevier.com/locate/rinp

# Two-photon bound–bound atomic transitions induced by LG beams

Ayman Al-Khateeb *, A. Lyras, V.E. Lembessis, O.M. Aldossary

*Quantum Technology Group, Department of Physics and Astronomy, College of Science, King Saud University, Riyadh 11451, Saudi Arabia*

ARTICLE INFO

*Keywords:*
Spin Angular Momentum (SAM)
Orbital Angular Momentum (OAM)
Laguerre Gaussian (LG)

ABSTRACT

We report theoretical results for the transition amplitudes of two-photon transitions induced in a one-active-electron atomic system by a $LG_{10}$ beam. We identify the excitation pathways for selected two-photon transitions starting from the ground state of the atomic system. We numerically evaluate these two-photon transition matrix elements for selected transitions in $Ca^{+}$ employing the truncated summation method. We provide a comparison with corresponding transitions induced by a Gaussian beam and present an estimation of the relative strength when the two different types of light beams are employed.

## Introduction

The polarization state of light waves was long ago recognized to be directly related to the optical Spin Angular Momentum (SAM) of electromagnetic waves In 1992, it was discovered that light possesses quantized Orbital Angular Momentum (OAM) by Allen et al [1] who demonstrated it in the laboratory by generating OAM-carrying light beams. Subsequently, intensive experimental and theoretical research, developed further and deepened the understanding of this concept, in addition to the development of many applications [2–6], like optical tweezers as a mechanical application [7–12], quantum communications and quantum cryptography [13–15], micro-manipulation [16], and spiral phase contrast imaging [17–19]. The ability to couple the OAM of light to the internal degrees of freedom of an atom was unambiguously and meticulously confirmed experimentally by Schmiegelow et al [20,21].

## Laguerre-Gaussian beams

Laguerre-Gaussian (LG) beams are an explicit demonstration of the OAM-carrying helical phase-fronts beams [3,22]. There are a number of other families of OAM-carrying beams [23–27]. In this work, we will be dealing only with LG beams.

LG beams are a family of solutions to the paraxial wave equation and their amplitude is given by [28]

$$u_{lp}^{LG}(\rho,\varphi,z)=\frac{C_p^{|l|}}{w(z)}\left(\frac{\sqrt{2}\,\rho}{w(z)}\right)^{|l|}\exp\left(\frac{-\rho^2}{w^2(z)}\right)L_p^{|l|}\left(\frac{2\rho^2}{w^2(z)}\right)\times exp\left(\frac{ik\rho^2 z}{2(z^2+z_R^2)}+il\varphi+i(2p+l+1)\arctan\left(\frac{z}{z_R}\right)\right) \tag{1.1}$$

where $u_{lp}^{LG}$ is written in cylindrical coordinates $(\rho,\varphi,z)$, $l\in\mathbb{Z}$ and $p\in\mathbb{N}_0$ are the azimuthal and radial integer indices, respectively, $w(z)=w_0\sqrt{1+z^2/z_R^2}$ is the usual beam radius at $z$, such that $z_R=\pi w_0^2/\lambda$ is the Rayleigh range, and $w_0$ is the beam waist at $z=0$. $L_p^{|l|}$ is the associated Laguerre polynomial, $c_p^{|l|}$ is the constant of normalization and $(2p+l+1)\arctan\left(\frac{z}{z_R}\right)$ is the Gouy phase.

The LG mode with $l=0$ and $p=0$ (Gaussian) is shown in Fig. 1(a). For $l\neq 0$ and $p=0$ the light intensity of the LG modes is ring-shaped and they are called donut modes (see Fig. 1(b),(c),(d)) [29].

## Light-Atom interaction

In our study, see Fig. 2, we consider a calcium ion $Ca^{+}$ (the red point) in the initial state $|i\rangle$ interacting with a light field defined by a vector potential $\vec{A}$ polarized in the x-direction and propagating in the z-direction that induces a transition to a final state $|f\rangle$.

For weak fields the Hamiltonian for the light-ion interaction is proportional to $\vec{A}\cdot\vec{p}+\vec{p}\cdot\vec{A}$ [30] and the applicable transition matrix element is [21]

* Corresponding author.
*E-mail address:* aalkhateeb@ksu.edu.sa (A. Al-Khateeb).

https://doi.org/10.1016/j.rinp.2022.106107
Received 14 September 2022; Received in revised form 24 October 2022; Accepted 11 November 2022
Available online 15 November 2022

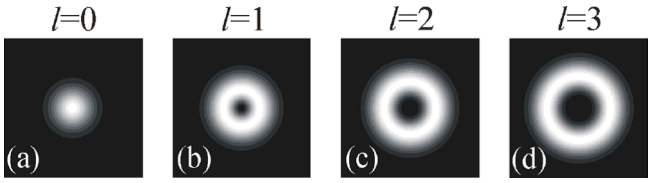


**Fig. 1.** LG modes and the transverse intensity profile with p = 0 and (a) $l = 0$, (b) $l = 1$, (c) $l = 2$, (d) $l = 3$.

$$\langle f|H_I|i\rangle \propto \left\langle f|\vec{A}\cdot\vec{p} + \vec{p}\cdot\vec{A}|i\right\rangle \propto \omega_{fi}\left\langle f|\vec{r}\cdot\vec{A}|i\right\rangle \tag{2.1}$$

Herein, for a certain purpose, $\vec{A}$ is a vector potential of Laguerre Gaussian beam with OAM [1] and we will use the cylindrical co-ordinates (ρ, φ, z) as we used for Eq. (1.1)

$$\vec{A}_{lp}(\rho,\varphi,z) = \vec{A}_0\sqrt{\frac{2p!}{\pi(|l|+p)!}}\left(\frac{\sqrt{2}\rho}{w(z)}\right)^{|l|}\frac{w_0}{w(z)}\,L_p^{|l|}\left(\frac{2\rho^2}{w^2(z)}\right)\times exp\left(ikz + il\varphi + \frac{ik\rho^2 z}{2(z^2+z_R^2)} - \frac{\rho^2}{w^2(z)} + i(2p+l+1)\arctan\left(\frac{z}{z_R}\right)\right) \tag{2.2}$$

In the case of a Gaussian beam, where $l = 0$ and $p = 0$, one can find that under such conditions [21] the expansion of the vector potential for the electric dipole and quadrupole approximations [31] is given by

$$\vec{A}_{00} \approx \vec{A}_0\,(1 + ikz) \tag{2.3}$$

where $\vec{A}_0$ is related to the dipole transition and the term $\vec{A}_0 ikz$ is responsible for the quadrupole transition.

Now for the Laguerre Gaussian beam such that $l = 1$ and $p = 0$ ($LG_{10}$), the leading term of the vector potential is

$$\vec{A}_{10} \approx \vec{A}_0\,\frac{\sqrt{2}\rho e^{i\varphi}}{w_0} \tag{2.4}$$

which as we will demonstrate below corresponds to the quadrupole approximation.

The calculation of the electric quadrupole transition matrix elements of the interaction Hamiltonian for the Gaussian beam can be written as follows:

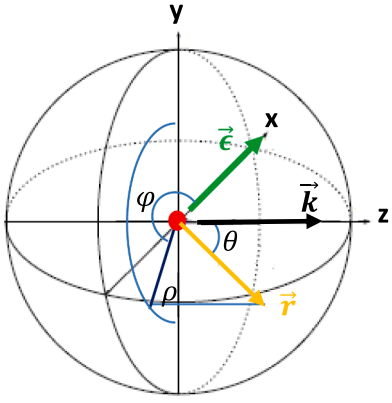


**Fig. 2.** A wave vector $\vec{k}$ of the laser beam propagates in z- direction while the linear polarization in the x-axis, and $\rho$ and $\vec{r}$ described by the polar angles $\varphi$ and $\theta$ respectively.

$$\begin{aligned}
\left\langle f|\ \vec{r}\cdot\vec{A}_{00}|i\right\rangle &= \left\langle f|\ \vec{r}\cdot\vec{A}_0\ ikz|i\ \right\rangle = ikA_0\langle f|xz|i\rangle \\
&= \frac{4\pi}{3}\sqrt{\frac{1}{2}}ikA_0\left\langle f|r^2\ \left(T_{-1}^{(1)} - T_{+1}^{(1)}\right)T_0^{(1)}|i\right\rangle \\
&= \frac{4\pi}{3}\sqrt{\frac{1}{2}}ikA_0\left\langle f|r^2\left(T_{-1}^{(1)}T_0^{(1)} - T_{+1}^{(1)}T_0^{(1)}\right)|i\right\rangle \\
&= \frac{4\pi}{3}\sqrt{\frac{1}{2}}ikA_0\left\langle f|r^2\left\{\sqrt{\frac{1}{2}}\left(T_{-1}^{(2)} - T_{-1}^{(1)}\right) - \sqrt{\frac{1}{2}}\left(T_{+1}^{(2)}\right.\right.\right. \\
&\quad \left.\left.\left. + T_{+1}^{(1)}\right)\right\}|i\right\rangle \\
&= \frac{2\pi}{3}ikA_0\left\langle f|r^2\left\{\left(T_{-1}^{(2)} - T_{-1}^{(1)}\right) - \left(T_{+1}^{(2)} + T_{+1}^{(1)}\right)\right\}|i\right\rangle
\end{aligned} \tag{2.5}$$

Further for $LG_{10}$

$$\begin{aligned}
\left\langle f|\ \vec{r}\cdot\vec{A}_{10}|i\right\rangle &= \left\langle f|\ \vec{r}\cdot\vec{A}_0\ \frac{\sqrt{2}\rho e^{i\varphi}}{w_0}|i\right\rangle = \frac{\sqrt{2}A_0}{w_0}\langle f|xrsin\theta e^{i\varphi}|i\rangle \\
&= \frac{-\sqrt{2}A_0}{w_0}\left\langle f|r^2\sqrt{\frac{1}{2}}\sqrt{\frac{4\pi}{3}}\ \left(T_{-1}^{(1)} - T_{+1}^{(1)}\right)\sqrt{\frac{8\pi}{3}}T_{+1}^{(1)}|i\right\rangle \\
&= \frac{4\pi}{3}\frac{\sqrt{2}A_0}{w_0}\left\langle f|r^2\left(T_{+1}^{(1)} - T_{-1}^{(1)}\right)T_{+1}^{(1)}|i\right\rangle \\
&= \frac{4\pi}{3}\frac{\sqrt{2}A_0}{w_0}\left\langle f|r^2\left(T_{+1}^{(1)}T_{+1}^{(1)} - T_{-1}^{(1)}T_{+1}^{(1)}\right)|i\ \right\rangle \\
&= \frac{4\pi}{3}\frac{\sqrt{2}A_0}{w_0}\left\langle f|r^2\left(T_{+2}^{(2)} + \frac{T_0^{(2)}}{\sqrt{6}} - \frac{T_0^{(1)}}{\sqrt{2}} + \frac{T_0^{(0)}}{\sqrt{3}}\right)|i\right\rangle
\end{aligned} \tag{2.6}$$

Eq. (2.6) represents only the interaction Hamiltonian of the transverse electric field with the atomic system. In 2017 a group of scientists from Argentina and Germany demonstrated that the longitudinal components of the electric field must be taken into account [32], in order to fully interpret the earlier experimental data [20], and that both transverse and longitudinal interaction components have comparable magnitudes and the ratio between them does not depend on the focal size. Moreover, they demonstrated that Eq. (2.6) must be modified into the following expanded form,

$$\left\langle f|\ \vec{r}\cdot\vec{A}_{10}|i\right\rangle = \frac{4\pi}{3}\frac{\sqrt{2}A_0}{w_0}\left\langle f|r^2\left(T_{+2}^{(2)} + \frac{3T_0^{(2)}}{\sqrt{6}} - \frac{T_0^{(1)}}{\sqrt{2}} + \frac{T_0^{(0)}}{\sqrt{3}}\right)|i\right\rangle \tag{2.7}$$

In deriving Eq. (2.5) and Eq. (2.7), we used certain expressions for the spherical tensor components as in the following equations,

$$\frac{z}{r} = \sqrt{\frac{4\pi}{3}}T_0^{(1)} \tag{2.8}$$

$$\frac{x}{r} = \sqrt{\frac{2\pi}{3}}\left(T_{-1}^{(1)} - T_{+1}^{(1)}\right) \tag{2.9}$$

$$sin\theta e^{i\varphi} = -\sqrt{\frac{8\pi}{3}}T_{+1}^{(1)} \tag{2.10}$$

$$T_{-1}^{(1)}T_0^{(1)} = \sqrt{\frac{1}{2}}\left(T_{-1}^{(2)} - T_{-1}^{(1)}\right) \tag{2.11}$$

$$T_{+1}^{(1)}T_0^{(1)} = \sqrt{\frac{1}{2}}\left(T_{+1}^{(2)} + T_{+1}^{(1)}\right) \tag{2.12}$$

$$T_{+1}^{(1)}T_{+1}^{(1)} = T_{+2}^{(2)} \tag{2.13}$$

$$T_{-1}^{(1)}T_{+1}^{(1)} = \frac{T_0^{(2)}}{\sqrt{6}} - \frac{T_0^{(1)}}{\sqrt{2}} + \frac{T_0^{(0)}}{\sqrt{3}} \tag{2.14}$$

**Two-Photon transitions**

In 1930 Maria Goeppert-Mayer suggested that $n$ photons each of energy hω can be absorbed to induce atomic transitions between two bound states with energy separation nhω, provided that the photons are arriving almost simultaneously withing a time interval considerably shorter than the excited state lifetime. More than 50 years ago, a lot of multiphoton transitions calculations on noble gases and alkali atoms have been performed [33–35]. In the seventies, many theoretical studies and experiments were conducted, which proved, among other things, that the polarization of the light affects the total multiphoton transition rates [36–38] while multiphoton ionization of atoms by polarized light can produce polarized photoelectrons if the spin–orbit coupling in the atomic species is exploited [39–41]. Of particular interest to our work here is the theoretical and experimental work on the dominant contribution in multiphoton ionization of quadrupole transitions when appropriate near-resonance excitations occur [42,43].

In our research, the results of which we present in detail below, we calculated the two-photon transition amplitudes for both Gaussian and $LG_{10}$ beams for specific transitions in $Ca^{+1}$ starting from its the ground state $4S_{\frac{1}{2}}$ . This one-active-electron ion has been employed in most of the recent literature on the interaction of LG beams with atomic systems. The expressions we derive can, of course, be applied to other one-active-electron systems, e.g. the alkaline atoms.

One of our goals was to identify the excitation channels through which these two-photon transitions proceed and compare the excitation pathways induced by Gaussian and LG beams, respectively. This comparison may become somewhat subtle, even in qualitative terms, so we tried our best to make it meaningful and relevant.

*Calculating two-photon transition amplitudes for Gaussian and* $\boldsymbol{LG_{10}}$ *beams*

The general formula for the transition amplitudes for two-photon transition is given by

$$T_{fi} = \sum_n \frac{\langle f|H_I|n\rangle\langle n|H_I|i\rangle}{E_n - E_i - E_l} \tag{3.1}$$

Here $|f\rangle$ is the final state, $|i\rangle$ is the initial state (always $4S_{\frac{1}{2}}$ in our study) and with spin–orbit coupling taken into account we use the LSJM state representation, so $|i\rangle = |0\,\frac{1}{2}\,\frac{1}{2}\,\frac{\pm 1}{2}\rangle$ , $|n\rangle$ is the intermediate state, $H_I$ is the interaction Hamiltonian and $E_n$, $E_i$, $E_l$ are the energies of the intermediate state, the initial state and the photon, respectively. In our study, we consider the interaction between the outer atomic electron in the state $4S_{\frac{1}{2}}$ and the Gaussian or $LG_{10}$ laser beam; so the interaction Hamiltonian $H_I$ is proportional to Eq. (2.5) (Gaussian $LG_{00}$) and/or Eq. (2.7) ($LG_{10}$). The electric quadrupole selection rules for both cases are.

(1) Parity is unchanged;
(2) ΔJ, ±1,±2; $J = 0 \leftrightarrow 0,\ 0 \leftrightarrow 1,\ 1/2 \leftrightarrow 1/2$ are not allowed;
(3) $\Delta M_J = 0, \pm 1, \pm 2$;
(4) $\Delta L = 0, \pm 1, \pm 2$; $L = 0 \leftrightarrow 0,\ 0 \leftrightarrow 1$ are not allowed;
(5) $\Delta S = 0$.

Substituting Eq. (2.5) into Eq. (3.1) we find the transition amplitude for a Gaussian ($LG_{00}$) beam

$$T_{fi}^{G} = \left(\frac{2\pi}{3} ikA_0\right)^2 \sum_n \frac{\left\langle f|r^2\left\{\left(T_{-1}^{(2)} - T_{-1}^{(1)}\right) - \left(T_{+1}^{(2)} + T_{+1}^{(1)}\right)\right\}|n\right\rangle \left\langle n|r^2\left\{\left(T_{-1}^{(2)} - T_{-1}^{(1)}\right) - \left(T_{+1}^{(2)} + T_{+1}^{(1)}\right)\right\}|i\right\rangle}{E_n - E_i - E_l} \tag{3.2}$$

And for a $LG_{10}$ beam using Eq. (2.7) into Eq. (3.1) we obtain

$$T_{fi}^{OAM} = \left(\frac{4\pi}{3}\frac{\sqrt{2}A_0}{w_0}\right)^2 \sum_n \frac{\left\langle f|r^2\left(T_{+2}^{(2)} + \frac{T_0^{(2)}}{\sqrt{6}} - \frac{T_0^{(1)}}{\sqrt{2}} + \frac{T_0^{(0)}}{\sqrt{3}}\right)|n\right\rangle \left\langle n|r^2\left(T_{+2}^{(2)} + \frac{T_0^{(2)}}{\sqrt{6}} - \frac{T_0^{(1)}}{\sqrt{2}} + \frac{T_0^{(0)}}{\sqrt{3}}\right)|i\right\rangle}{E_n - E_i - E_l} \tag{3.3}$$

With an initial state $4S_{\frac{1}{2}}$ (S = 1/2, L = 0, and J = 1/2) and final states of symmetry $S$, $D$, $G$, taking into account the electric quadrupole selection rules, the transition matrix elements for $T_0^{(0)}$ *and* $T_{\pm 1,0}^{(1)}$ are zero.

Therefore Eq. (3.2) and Eq. (3.3) simplify to

$$T_{fi}^{G} = \left(\frac{4\pi^2}{9} k^2 A_0^2\right) \sum_n \frac{\left\langle f|r^2\left\{T_{+1}^{(2)} - T_{-1}^{(2)}\right\}|n\right\rangle \left\langle n|r^2\left\{T_{+1}^{(2)} - T_{-1}^{(2)}\right\}|i\right\rangle}{E_n - E_i - E_l} \tag{3.4}$$

$$T_{fi}^{OAM} = \left(\frac{4\pi}{3}\frac{\sqrt{2}A_0}{w_0}\right)^2 \sum_n \frac{\left\langle f|r^2\left(T_{+2}^{(2)} + \frac{3T_0^{(2)}}{\sqrt{6}} - \frac{T_0^{(1)}}{\sqrt{2}}\right)|n\right\rangle \left\langle n|r^2\left(T_{+2}^{(2)} + \frac{3T_0^{(2)}}{\sqrt{6}} - \frac{T_0^{(1)}}{\sqrt{2}}\right)|i\right\rangle}{E_n - E_i - E_l} \tag{3.5}$$

Considering Eq. (3.4) and Eq. (3.5), one can see that:

(i) For the two-photon absorption, the transition occurs if the sum of the total angular momentum of the two photons $(m_T = m_{ph1} + m_{ph2})$ matches the change in the projection angular momentum $\Delta m_j$ between the initial and the final state.

(ii) The linearly polarized light is a superposition of right circularly polarized (SAM=+1) and left circularly polarized (SAM = -1). Moreover, the light in a Gaussian beam $LG_{00}$ has OAM = 0 while for a $LG_{10}$ OAM= + 1, in our calculations. Therefore, for the linearly polarized Gaussian beam the total magnetic angular momentum of the two photons could be $m_T = -2\ ,\ 0\ and +2$ and for the linearly polarized $LG_{10}$ beam total angular momentum of the two photons could be $m_T = 0\ ,\ +2\ and\ +4$. These quantum numbers, according to remark (i) above, define the allowed two-photon transitions while transitions for which $m_T \neq \Delta m_j$ are forbidden.

## Results

The volume of the formal results we obtained is significant. We included a detailed list of our results together with detailed excitation diagrams that describe the two-photon transition pathways in the Supplementary Material file. In this section, we will present just two representative cases in order to discuss the formal structure of our results and facilitate the discussion in the following section.

At first, let us consider a two-photon transition from the $4S_{1/2}$ initial state to the $6S_{1/2}$ final state. For a Gaussian beam, considering only quadrupole transitions, we obtain

$$T_{4S\to 6S} = \left(\frac{4\pi^2}{9}k^2A_0^2\right)\left\{\frac{1}{10\pi}(2S_{13} + 3S_{14})\right\} \tag{4.1}$$

where the two-photon transition amplitudes $S_{ij}$, that result from the summation over all symmetry-allowed intermediate states, are given by the following expressions:

$$S_{13} = \sum_n \frac{\left(R^{50\left(\frac{1}{2}\right)}_{n2\left(\frac{3}{2}\right)} R^{n2\left(\frac{3}{2}\right)}_{40\left(\frac{1}{2}\right)}\right)}{E_{|n2\frac{1}{2}\frac{3}{2}\rangle} - E_{|40\frac{1}{2}\frac{1}{2}\rangle} - E_l} \tag{4.2}$$

$$S_{14} = \sum_n \frac{\left(R^{50\left(\frac{1}{2}\right)}_{n2\left(\frac{5}{2}\right)} R^{n2\left(\frac{5}{2}\right)}_{40\left(\frac{1}{2}\right)}\right)}{E_{|n2\frac{1}{2}\frac{5}{2}\rangle} - E_{|40\frac{1}{2}\frac{1}{2}\rangle} - E_l} \tag{4.3}$$

where

$$R^{n'l'(j')}_{nl(j)} = \int_0^\infty r^2 dr\ \ R_{n'l'}(r)\ r^2\ R_{nl}(r) \tag{4.4}$$

are the appropriate radial matrix elements for the symmetry-allowed transitions.

At this point it is necessary to comment on our choice to consider only quadrupole transitions in the calculation of the two-photon transition matrix element given in Eq. (4.1). It is true that the transition can be induced in the dipole approximation and as is well known in the literature it will dominate the transition discussed herein by many orders of magnitude. However, it seems a reasonable assumption to disregard dipole-allowed transitions for a meaningful comparison with the results obtained using a $LG_{10}$ field since almost all the relevant literature so far has associated these fields with quadrupole transitions. Moreover, in the case the first photon is in near resonance with a dipole-forbidden transition the result shown in (4.1) will be the dominant contribution to the two-photon transition probability.

Considering the same two-photon transition induced by a $LG_{10}$ field, we obtain the following expression,

$$T^{LG}_{4S\to 6S} = \frac{32\pi^2}{9}\frac{{A_0}^2}{{w_0}^2}\left\{\frac{1\times 9}{120\pi}(2S_{13} + 3S_{14}) + \frac{1}{24\pi}(S_1 + 2S_2)\right\} \tag{4.5}$$

where $w_0$ is the beam waist. The two-photon transition amplitudes that appear in (4.5) in the term highlighted in red are defined as,

$$S_1 = \sum_n \frac{\left(R^{52\left(\frac{1}{2}\right)}_{n1\left(\frac{1}{2}\right)} R^{n1\left(\frac{1}{2}\right)}_{40\left(\frac{1}{2}\right)}\right)}{E_{|n1\frac{1}{2}\frac{1}{2}\rangle} - E_{|40\frac{1}{2}\frac{1}{2}\rangle} - E_l} \tag{4.6}$$

$$S_2 = \sum_n \frac{\left(R^{52\left(\frac{1}{2}\right)}_{n1\left(\frac{3}{2}\right)} R^{n1\left(\frac{3}{2}\right)}_{40\left(\frac{1}{2}\right)}\right)}{E_{|n1\frac{1}{2}\frac{3}{2}\rangle} - E_{|40\frac{1}{2}\frac{1}{2}\rangle} - E_l} \tag{4.7}$$

The numerical factor highlighted in green results from the transverse component of the interaction Hamiltonian and as it was to be expected from the earlier applications of this term in calculating one-photon transitions, it contributes to an enhancement (by almost an order of magnitude) of the corresponding component of the transition matrix element. The term highlighted in red represents the contribution of dipole-allowed transitions that are induced by the $T_0^{(1)}$ operator in (3.5). Therefore, it becomes now clear that in order to have a meaningful comparison, at least theoretically, between results obtained with Gaussian and $LG_{10}$ fields, one has to include in the Gaussian case both the dipole and the quadrupole interaction terms. This means that in Eq. (4.1) an additional term would be included; formally similar to the one in the bracket highlighted in red in Eq. (4.5) the only difference being the overall numerical prefactor. The preceding discussion clarifies the context in which meaningful comparisons between two-photon transitions induced by Gaussian and $LG_{10}$ fields can be made, at least theoretically.

The preceding discussion can be extended to all the results included in detail in the Supplementary Material file. It is worth noting that when the final state is of $G$ symmetry dipole-allowed channels do not contribute to the two-photon matrix element. Such transitions may be a favorable target for future experimental investigations of two-photon transitions induced by $LG_{10}$ fields. The analysis of the experimental data could be based on the results derived and tabulated in this work.

## Numerical examples

The numerical calculation of two-photon matrix elements is a conceptually non-trivial and computationally intensive task. However, it is interesting to, at least, attempt a reasonably accurate numerical calculation of such matrix elements when LG beams are involved in order to gain some understanding on the relative orders of magnitude.

We will present our approach using as a typical example a two-photon matrix element for transitions induced by a Gaussian ($LG_{00}$) beam. The approach is exactly the same for all other matrix elements we calculated numerically.

The formal expression for the two-photon matrix element from $4S_{1/2}$ to $6S_{1/2}$ is

$$T_{4S\to 6S} = \left(\frac{4\pi^2}{9}k^2A_0^2\right)\left\{\frac{1}{10\pi}(2S_{13} + 3S_{14})\right\} \tag{5.1}$$

where,

$$S_{13} = \sum_n \frac{\left(R^{50\left(\frac{1}{2}\right)}_{n2\left(\frac{3}{2}\right)} R^{n2\left(\frac{3}{2}\right)}_{40\left(\frac{1}{2}\right)}\right)}{E_{|n2\frac{1}{2}\frac{3}{2}\rangle} - E_{|40\frac{1}{2}\frac{1}{2}\rangle} - E_l} \tag{5.2}$$

$$S_{14} = \sum_n \frac{\left(R^{50\left(\frac{1}{2}\right)}_{n2\left(\frac{5}{2}\right)} R^{n2\left(\frac{5}{2}\right)}_{40\left(\frac{1}{2}\right)}\right)}{E_{|n2\frac{1}{2}\frac{5}{2}\rangle} - E_{|40\frac{1}{2}\frac{1}{2}\rangle} - E_l} \tag{5.3}$$

The computational task is the numerical evaluation of $S_{13}$ and $S_{14}$ , which can be split in two parts. The first part, which is the simpler one, is the calculation of the radial matrix elements

$$R^{nl}_{n'l'} = \int_0^\infty r^2 dr \;\; R_{n'l'}(r)\; r^2\; R_{nl}(r) \tag{5.4}$$

In particular, in order to calculate $S_{13}$ and $S_{14}$ one has to evaluate the integrals $R^{50\left(\frac{1}{2}\right)}_{n2\left(\frac{3}{2}\right)}$ *and* $R^{n2\left(\frac{3}{2}\right)}_{40\left(\frac{1}{2}\right)}$ where

$$R^{50\left(\frac{1}{2}\right)}_{n2\left(\frac{3}{2}\right)} = \int_0^\infty r^2 dr \;\; R_{50}(r)\; r^2\; R_{n2}(r)$$

and

$$R^{n2\left(\frac{3}{2}\right)}_{40\left(\frac{1}{2}\right)} = \int_0^\infty r^2 dr \;\; R_{n2}(r)\; r^2\; R_{40}(r)$$

Where $n$ is the principal quantum number (for $Ca^+$, $n \geqslant 3$), and $R_{nl}(r)$ is the normalized radial wave function of the Hydrogen-like ion,

$$R_{nl}(r) = -\sqrt{\left(\frac{2Z}{na_\mu}\right)^3 \frac{(n-l-1)!}{2n(n+l)!}} e^{-\frac{Zr}{na_\mu}} \left(\frac{2Zr}{na_\mu}\right)^l L^{(2l+1)}_{n-l-1}\left(\frac{2Zr}{na_\mu}\right) \tag{5.5}$$

where $L^{(2l+1)}_{n-l-1}$ are the generalized Laguerre polynomials, $a_\mu = \frac{m_e}{\mu} a_0$, with $\mu = \frac{m_e m_N}{m_e + m_N}$ the reduced mass, $m_N$ the mass of the nucleus and $a_0$ the Bohr radius. Hence, for $Ca^+$, Z = 20 and $a_\mu = 5.29184 \times 10^{-11}$ m. These radial wavefunctions do not include any fine-structure effects and do not depend on $J$; the labels in brackets are only used in order to keep track of the terms in the summations over intermediate states. The numerical values of the radial integrals, like $R^{50\left(\frac{1}{2}\right)}_{n2\left(\frac{3}{2}\right)}$ for example, are obtained using the Wolfram Alpha online integration software facility (https://www.wolframalpha.com/). These results are tabulated along with other numerical values in the Supplementary Material file.

The second part of the computational task is to perform the infinite summations over intermediate states that are allowed from angular momentum selection rules. The straightforward, although not necessarily the most accurate, approach is to include in the summation intermediate states for which experimental energy values have been obtained and tabulated; this is the so-called truncated summation approach. Under certain circumstances the numerical results may be quite reliable, for example when one of the intermediate states included in the summation is in near-resonance with the ground state. When the number of intermediate states included in the summation is sufficiently large it is possible to conduct convergence tests to verify the numerical accuracy of the calculation. In any case, this approach neglects the contribution of the continuum spectrum in the summation which may be significant if in the contribution of the bound spectrum cancellations occur between terms with opposite signs, resulting either from the signs of the energy denominators or the ones of the radial matrix elements.

As a first attempt at obtaining numerical results for the two-photon matrix elements we derived, we employed the truncated summation approach using $Ca^+$ as our model one-electron system, since it has been used in most of the literature so far. We used the energy level values given in [44]. In this approach the effect of the fine-structure of the atomic system is taken into account through the angular momentum selection rules and the experimental energy values for the intermediate states. We have tabulated, as meticulously as possible, all our numerical results in Tables S8–S21 in the Supplementary Material file.

Browsing through the tables some general conclusions can be drawn. The matrix elements for which intermediate states of $P$ symmetry are involved, were calculated with only three intermediate states because of lack of corresponding experimental data. On the contrary, the matrix elements with $D$-symmetry intermediate states were calculated using 10 intermediate states and are deemed to be more accurate, within the limits of the employed approach. There is certainly room for improvement in the accuracy of the numerical results. One approach could be to employ the Green's function approach in the context of single-channel quantum defect theory. It will be one of our future research goals to employ such an approach for a host of one-electron systems, including alkali atoms. The numerical results suggest that for the atomic species we studied and within the limits of the employed computational approach, the $S_{ij}$ matrix elements, like the ones shown in (5.2) and (5.3), have roughly the same order of magnitude both for Gaussian and $LG_{10}$ beams. As a final remark, let us attempt to estimate the relative strength of the two-photon transitions induced by Gaussian and $LG_{10}$ beams respectively. We could use Eq. (3.4) and Eq. (3.5) and the results tabulated in the Supplementary Material file. Then it is evident that for $\Delta m_j = 0$ transitions, the ratio of Gaussian to $LG_{10}$ is $\sim \frac{\pi^2 w_0^2}{2\lambda^2}$, where $w_0$ is the beam waist and $\lambda$ is the wavelength of the light beam. C.T Schmiegelow et al [20] used a laser beam with $w_0 = 2.7\mu m$ and $\lambda = 729\ nm$ and they measured that this ratio for a one-photon quadrupole transition is approximately 13.0. For the two-photon transition $4S_{\frac{1}{2}}$ to $6S_{\frac{1}{2}}$ in $Ca^+$ the photon wavelength is 283 *nm*. So using the values for the beam waist and the wavelength to be 2.7 $\mu m$ and 283 *nm* respectively, we estimate this ratio to be about $4.5 \times 10^2$ for two-photon transitions, i.e. approximately an order of magnitude larger than for one-photon transitions.

## Conclusions and discussion

We report detailed theoretical calculations of specific two-photon transitions induced by a $LG_{10}$ field in a one-active electron atomic system. We also report similar transition matrix elements for a Gaussian beam. We clarify the context within which such theoretical calculations may be meaningfully compared and we underline the importance of including dipole-allowed transition channels in the calculation of the two-photon transition amplitudes. We report numerical results for selected two-photon transitions in $Ca^+$ employing the truncated summation method and offer an estimate for the relative magnitude of two-photon transitions induced by Gaussian and $LG_{10}$ beams, respectively.

Our results are a first attempt at addressing the question of two-photon transitions induced by OAM-carrying light beams. A number of variations in and additions to our study could include $LG$ beams with different indices (both $l$ and $p$) as well as different two-photon atomic transitions allowed by the selection rules. Numerical calculations of two-photon transition amplitudes of improved and controllable accuracy in a variety of one-electron atoms would be also desirable but in our opinion this tedious and non-trivial exercise would be more meaningful in the context of a concerted experimental and theoretical investigation. Such an investigation will also reveal the possible limitations of the theoretical approach developed in the present study as well as unforeseen advantages in using OAM-carrying beams for two-photon transitions. Another interesting aspect of such interactions that has recently emerged as a promising research direction, is the spatial dependence of selection rules and transition rates when the atomic system is located (presumably by optical traps or tweezers) at an off-axis position [45,46]. In the context of two-photon transitions the spatial dependence will be particularly complex because of the product of two single-photon matrix elements appearing in the numerator of the infinite summation over intermediate states. One may have to resort to a fully numerical calculation in order to produce specific results for the spatial dependence of the two-photon transition matrix elements. It is a topic we plan to pursue in a future study.

## Declaration of Competing Interest

The authors declare that they have no known competing financial interests or personal relationships that could have appeared to influence the work reported in this paper.

## Data availability

Data will be made available on request.

## Appendix A. Supplementary data

Supplementary data to this article can be found online at https://doi.org/10.1016/j.rinp.2022.106107.

## References


[1] Allen L, Beijersbergen MW, Spreeuw RJC, Woerdman JP. Orbital angular momentum of light and the transformation of Laguerre-Gaussian laser modes. Phys Rev A 1992;45(11):8185–9.
[2] Allen L, Padgett MJ, Babiker IV M. The orbital angular momentum of light. Prog Opt 1999;39:291–372.
[3] Allen L, Barnett SM, Padgett MJ. *Optical angular momentum*; CRC press, 2016; ISBN 0429174942.
[4] Andrews, D.L. *Structured light and its applications: An introduction to phase-structured beams and nanoscale optical forces*; Academic press, 2011; ISBN 0080559662.
[5] Torres, J.P.; Torner, L. *Twisted photons: applications of light with orbital angular momentum*; John Wiley & Sons, 2011; ISBN 3527635378.
[6] Andrews DL, Babiker M, editors. The Angular Momentum of Light. Cambridge University Press; 2012.
[7] He H, Friese MEJ, Heckenberg NR, Rubinsztein-Dunlop H. Direct observation of transfer of angular momentum to absorptive particles from a laser beam with a phase singularity. Phys Rev Lett 1995;75:826.
[8] Friese MEJ, Nieminen TA, Heckenberg NR, Rubinsztein-Dunlop H. Optical alignment and spinning of laser-trapped microscopic particles. Nature 1998;394:348–50.
[9] Clifford MA, Arlt J, Courtial J, Dholakia K. High-order Laguerre-Gaussian laser modes for studies of cold atoms. Opt Commun 1998;156:300–6.
[10] Dholakia K, MacDonald M, Spalding G. Optical tweezers: the next generation. Phys world 2002;15(10):31–5.
[11] Grier DG. A revolution in optical manipulation. Nature 2003;424(6950):810–6.
[12] Ladavac K, Grier DG. Microoptomechanical pumps assembled and driven by holographic optical vortex arrays. Opt Express 2004;12:1144–9.
[13] Yao AM, Padgett MJ. Orbital angular momentum: origins, behavior and applications. Adv Opt photonics 2011;3:161–204.
[14] Mirhosseini M, Magaña-Loaiza OS, O'Sullivan MN, Rodenburg B, Malik M, Lavery MPJ, et al. High-dimensional quantum cryptography with twisted light. New J Phys 2015;17:33033.
[15] Wang J. Advances in communications using optical vortices. Photonics Res 2016;4:B14–28.
[16] Galajda P, Ormos P. Complex micromachines produced and driven by light. Appl Phys Lett 2001;78:249–51.
[17] Fürhapter S, Jesacher A, Bernet S, Ritsch-Marte M. Spiral interferometry. Opt Lett 2005;30:1953–5.
[18] Züchner T, Failla AV, Meixner AJ. Light microscopy with doughnut modes: a concept to detect, characterize, and manipulate individual nanoobjects. Angew Chemie Int Ed 2011;50:5274–93.
[19] Baránek M, Bouchal Z. Rotating vortex imaging implemented by a quantized spiral phase modulation. J Eur Opt Soc Publ 2013;8.
[20] Schmiegelow CT, Schulz J, Kaufmann H, Ruster T, Poschinger UG, Schmidt-Kaler F. Transfer of optical orbital angular momentum to a bound electron. Nat Commun 2016;7:1–6.
[21] Schmiegelow CT, Schmidt-Kaler F. Light with orbital angular momentum interacting with trapped ions. Eur Phys J D 2012;66:1–9.
[22] Padgett M, Courtial J, Allen L. Light's orbital angular momentum. Phys Today 2004;57:35–40.
[23] Garcés-Chávez V, McGloin D, Padgett MJ, Dultz W, Schmitzer H, Dholakia K. Observation of the transfer of the local angular momentum density of a multiringed light beam to an optically trapped particle. Phys Rev Lett 2003;91:93602.
[24] McGloin D, Dholakia K. Bessel beams: diffraction in a new light. Contemp Phys 2005;46:15–28.
[25] Courtial J, Dholakia K, Allen L, Padgett MJ. Second-harmonic generation and the conservation of orbital angular momentum with high-order Laguerre-Gaussian modes. Phys Rev A 1997;56(5):4193–6.
[26] Bandres MA, Gutiérrez-Vega JC. Ince–gaussian beams. Opt Lett 2004;29:144–6.
[27] Kotlyar VV, Skidanov RV, Khonina SN, Soifer VA. Hypergeometric modes. Opt Lett 2007;32:742–4.
[28] Romero LCD, Andrews DL, Babiker M. A quantum electrodynamics framework for the nonlinear optics of twisted beams. J Opt B Quantum Semiclassical Opt 2002;4:S66.
[29] Morris JE. Studies of novel beam shapes and applications to optical manipulation. University of St Andrews; 2010. Diss.
[30] Gasiorowicz, S. *Quantum physics*; John Wiley & Sons, 2007; ISBN 8126511176.
[31] Sakurai JJ, Tuan SF, Commins ED. Modern Quantum Mechanics, Revised Edition. Am J Phys 1995;63(1):93–5.
[32] Quinteiro GF, Schmidt-Kaler F, Schmiegelow CT. Twisted-light–ion interaction: the role of longitudinal fields. Phys Rev Lett 2017;119:253203.
[33] Bebb HB, Gold A. Multiphoton ionization of hydrogen and rare-gas atoms. Phys Rev 1966;143:1.
[34] Bebb HB. Quantitative theory of the two-photon ionization of the alkali atoms. Phys Rev 1966;149:25.
[35] Bebb HB. Theory of three-photon ionization of the alkali atoms. Phys Rev 1967;153:23.
[36] Fox RA, Kogan RM, Robinson EJ. Laser triple-quantum photoionization of cesium. Phys Rev Lett 1971;26:1416.
[37] Lambropoulos P. Effect of light polarization on multiphoton ionization of atoms. Phys Rev Lett 1972;28:585.
[38] Cervenan MR, Isenor NR. Three-photon ionization cross-section of potassium for single-mode ruby laser radiation. Opt Commun 1974;10:280–2.
[39] Lambropoulos P. Spin-orbit coupling and photoelectron polarization in multiphoton ionization of atoms. Phys Rev Lett 1973;30:413.
[40] Farago PS, Walker DW. Two-photon ionization of trivalent atoms as a source of polarized electrons. J Phys B At Mol Phys 1973;6:L280.
[41] Jacobs VL. Polarization phenomena in multiphoton ionization of atoms. J Phys B At Mol Phys 1973;6:1461.
[42] Lambropoulos P, Doolen G, Rountree SP. Electric quadrupole transitions in multiphoton ionization. Phys Rev Lett 1975;34:636.
[43] Lambropoulos M, Moody SE, Smith SJ, Lineberger WC. Observation of electric quadrupole transitions in multiphoton ionization. Phys Rev Lett 1975;35:159.
[44] Sugar J, Corliss C. Energy levels of calcium, Ca I through Ca XX. J Phys Chem Ref Data 1979;8(3):865–916.
[45] Afanasev A, Carlson CE, Schmiegelow C, Schulz J, Schmidt-Kaler F, Solyanik M. Experimental verification of position-dependent angular-momentum selection rules for absorption of twisted light by a bound electron. New J Phys 2018;20:023032.
[46] Solyanik-Gorgone M, Afanasev A, Carlson CE, Schmiegelow C, Schmidt-Kaler F. Excitation of E1-forbidden transitions with electric, magnetic, and mixed multipolarity in light fields carrying orbital and spin angular momentum. J Opt Soc Am B 2019;30:565–74.